

# Dynamics of collapsing and exploding Bose-Einstein condensates

Elizabeth A. Donley, Neil R. Claussen, Simon L. Cornish, Jacob L. Roberts, Eric A. Cornell\* and Carl E. Wieman  
*JILA, National Institute of Standards and Technology and the University of Colorado,  
and the Department of Physics, University of Colorado, Boulder, Colorado 80309-0440*  
(Dated: December 2, 2024)

We explored the dynamics of how a Bose-Einstein condensate collapses and subsequently explodes when the balance of forces governing the size and shape of the condensate is suddenly altered. A condensate's equilibrium size and shape is strongly affected by the inter-atomic interactions. Our ability to induce a collapse by switching the interactions from repulsive to attractive by tuning an externally-applied magnetic field yields a wealth of detailed information on the violent collapse process. We observe anisotropic atom bursts that explode from the condensate, atoms leaving the condensate in undetected forms, spikes appearing in the condensate wave function, and oscillating remnant condensates that survive the collapse. These all have curious dependencies on time, the strength of the interaction, and the number of condensate atoms. Although ours would seem to be a simple well-characterized system, our measurements reveal many interesting phenomena that challenge theoretical models.

A variety of phenomena in atomic Bose-Einstein condensates are affected by the interactions between the atoms. The vast majority of these phenomena are well described by mean-field theory<sup>1</sup>, in which the strength of the interactions depends on the atom density and on one additional parameter called the *s*-wave scattering length *a*. *a* is determined by the atomic species. When *a* > 0, the interactions are repulsive. In contrast, when *a* < 0 the interactions are attractive and a Bose-Einstein condensate (BEC) tends to contract to reduce its overall energy. In a harmonic trap, the contraction competes with the kinetic zero-point energy, which tends to spread out the condensate. For a strong enough attractive interaction, there is not enough kinetic energy to stabilize the BEC and it is expected to implode. A BEC can avoid implosion only as long as the number of atoms *N*<sub>0</sub> is less than a critical value given by<sup>2</sup>

$$N_{cr} = ka_{ho}/|a|, \quad (1)$$

where dimensionless constant *k* is called the stability coefficient. *a*<sub>ho</sub> is the harmonic oscillator length, which sets the size of the condensate in the ideal-gas (*a* = 0) limit.

Under most circumstances, *a* is insensitive to external fields. This is different in the vicinity of a so-called Feshbach resonance, where *a* can be tuned over a huge range by adjusting the externally applied magnetic field. For <sup>85</sup>Rb atoms *a* is usually negative, but a Feshbach resonance at ~155 G allows us to tune *a* by orders of magnitude and even change its sign. This gives us the ability to create stable <sup>85</sup>Rb Bose-Einstein condensates<sup>3</sup> and adjust the inter-atomic interactions. We recently used this flexibility to verify the functional form of equation (1) and to measure the stability coefficient to be *k* = 0.46(6)<sup>4</sup>.

In this article, we study the dynamical response (“the collapse”) of an initially stable BEC to a sudden shift of the scattering length to a value more negative than the critical value *a*<sub>cr</sub> = -*k**a*<sub>ho</sub>/*N*<sub>0</sub>. We have observed many features of the surprisingly complex collapse process, including the energies and energy anisotropies of atoms that burst from the condensate, the time scale for

the onset of this burst, the rates for losing atoms, spikes in the wave function that form during collapse, and the size of the remnant BEC that survives the collapse. The unprecedented level of control provided by tuning *a* has allowed us to see how all of these quantities depend on the magnitude of *a*, the initial number and density of condensate atoms, and the initial spatial size and shape of the BEC before the transition to instability.

We compare our measurements to various theoretical treatments of this problem<sup>5,6,7,8,9</sup>. A great deal of theoretical interest was generated by BEC experiments in <sup>7</sup>Li, for which the scattering length is also negative<sup>10,11</sup>. The <sup>7</sup>Li experiments do not employ a Feshbach resonance, so *a* is fixed. This restricts experimentation to the regime where the initial number of condensate atoms is less than or equal to *N*<sub>cr</sub>, and the collapse is driven by a stochastic process. In addition, studies of collapse dynamics in <sup>7</sup>Li are complicated by a large thermal component. Our ability to tune the scattering length, and most notably explore the regime where the initial condensate is “pure” (near *T* = 0) and the number *N*<sub>0</sub> is much larger than *N*<sub>cr</sub>, allows us to explore the dynamics and compare it with theory in far more detail.

**Experimental techniques.** The procedure for producing stable <sup>85</sup>Rb condensates has been described in detail elsewhere<sup>3</sup>. A standard double magneto-optical trap (MOT) system<sup>12</sup> was used to collect a cold sample of <sup>85</sup>Rb atoms in a low-pressure chamber. Once sufficient atoms had accumulated in the low-pressure MOT, the atoms were loaded into a cylindrically symmetric cigar-shaped magnetic trap<sup>13</sup>. Radio-frequency evaporation was then used to cool the sample to ~3 nK to form pure condensates containing >90% of the sample atoms. The final stages of evaporation were performed at 162 G where the scattering length is positive and stable condensates of up to 15,000 atoms could be formed. After evaporative cooling, the magnetic field was ramped adiabatically to 166 G (except where noted), where *a* = 0. This provided a well-defined initial condition with the BEC taking on the size and shape of the harmonic oscillator ground

state.

We could then adjust the mean-field interactions within the BEC to a variety of values on time scales as short as 0.1 ms. The obvious manipulation was to jump to some value of  $a < a_{cr}$  to trigger a collapse, but the tunability of  $a$  also greatly aided in imaging the sample. Usually the condensate size was below the resolution limit of our imaging system ( $7\mu\text{m}$  FWHM). However, we could ramp the scattering length to large positive values and use the repulsive inter-atomic interactions to expand the BEC before imaging, thus obtaining information on the pre-expansion condensate shape and number. A typical  $a(t)$  sequence is shown in Fig. 1a. We have used a variety of such sequences to explore many aspects of the collapse and enhance the observation of particular components of the sample.

**Condensate contraction and atom loss.** When the scattering length is jumped to a value  $a_{collapse} < a_{cr}$ , a condensate's kinetic energy no longer provides a sufficient barrier against collapse. As described in ref. 5, during collapse one might expect a BEC to contract until losses from density-dependent inelastic collisions<sup>14</sup> would effectively stop the contraction. This contraction would roughly take place on the time scale of a trap oscillation, and the density would sharply increase after  $T_{rad}/4 \simeq 14$  ms, where  $T_{rad}$  is the radial trap period. How does this picture compare to what we have actually seen?

A plot of the condensate number  $N$  vs  $\tau_{evolve}$  for  $a_{collapse} = -30 a_0$  and  $a_{init} = +7 a_0$  is presented in Fig. 1b.  $N$  was constant for some time after the jump until atom loss suddenly began at  $t_{collapse}$ . After the jump the condensate was smaller than our resolution limit, so we could not observe the contraction directly. But we observed that the post-expansion condensate widths changed very little with time  $\tau_{evolve}$  before  $t_{collapse}$ <sup>15</sup>. From this we infer that the bulk BEC did not contract dramatically before loss began. We modelled the contraction by approximating the BEC by a Gaussian wave function<sup>16</sup> and applying the  $a(t)$  sequence that we used for the experiment. The model predicted that by  $t_{collapse}$ , the radial and axial widths had contracted by  $\sim 20\%$  and  $\sim 4\%$ , respectively, from their initial values. This contraction only corresponds to a 50% increase in the average density to  $5 \times 10^{13}/\text{cm}^3$ , which is far too small to explain the observed decay constant  $\tau_{decay}$  by the inelastic collision picture of ref. 5.

For the data in Fig. 1b and most other data presented below, we jumped to  $a_{quench} = 0$  in 0.1 ms after a time  $\tau_{evolve}$  at  $a_{collapse}$ . We believe that the loss immediately stopped after the jump. This interpretation is based on the surprising observation that the quantitative details of curves such as that shown in Fig. 1b did not depend on whether the collapse was terminated by a jump to  $a_{quench} = 0$  or  $a_{quench} = 250 a_0$ .

We have measured loss curves like that in Fig. 1b for many different values of  $a_{collapse}$ . The collapse time versus  $a_{collapse}$  for  $N_0 = 6000$  is presented in Fig. 2. In addition to the strong dependence on  $a_{collapse}$ , the

collapse time was also sensitive to the initial scattering length<sup>17</sup> and the initial density, and increased with decreasing density. The atom loss time constant  $\tau_{decay}$  only weakly depended on  $a_{collapse}$  and  $N_0$ <sup>18</sup>.

**Burst atoms.** As indicated by Fig. 1b, atoms leave the BEC during the collapse. There are at least two components to the expelled atoms. One component (the “missing atoms”) is not detected. The other component emerges as a burst of detectable spin-polarized atoms with energies much greater than the initial condensate's energy but much less than the magnetic trap depth. The burst-energy dependencies on  $a_{collapse}$  and  $N_0$  are complex, but since they will provide a stringent test of collapse theories, we present them in detail.

The angular kinetic-energy distribution with which the burst atoms are expelled from the condensate can most accurately be measured by observing their harmonic oscillations in the trap, as illustrated in Fig. 3a. For example, half of a radial period after the expulsion ( $T_{rad}/2$ ), all atoms return to their initial radial positions. Well before or well after this “radial focus”, the burst cloud is too dilute to be observed. Fortunately, at the radial focus, oscillations along the axial trap axis are near their outer turning points and the axial energy can be found from the length of the stripe of atoms along the axial axis. The radial energy can be found with the same procedure for an axial focus. The sharpness of the focus also provides information on the time extent of the burst.

Figure 3b shows an image of a radial focus. The size scales for the burst focus and the remnant were well separated since the latter was not expanded before imaging. Figure 3c shows cross sections of the burst focus and fits to the burst and the thermal cloud. The burst energy distributions were well fit by Gaussians characterized by a temperature that was usually different for the two trap directions. The burst energy fluctuated from shot to shot by up to a factor of 2 for a given  $a_{collapse}$  (the measurement uncertainty was only  $\sim 10\%$ ), but the average value showed clear trends. The axial and radial burst energies versus  $a_{collapse}$  are shown in Fig. 4a and 4b for  $N_0 = 6,000$  and  $15,000$ , respectively. The burst-energy anisotropy shown in Fig. 4c depended on  $N_0$ ,  $a_{collapse}$ , and  $a_{init}$ .

The bursts were not emitted instantaneously. For the conditions of Fig. 1b, the number of burst atoms  $N_{burst}$  grew with  $\tau_{evolve}$  with a time constant of 1.2 ms starting at 3.5 ms and reaching an asymptotic final number of  $\sim 2500$  for all times  $\geq 7$  ms.  $N_{burst}$  varied randomly by  $\sim 20\%$  for the data in Fig. 4, but on average the fraction of atoms going into the burst was about 20% of  $N_0$  and did not depend on  $a_{collapse}$  or  $N_0$ .

**Remnant Condensate.** After a collapse, a “remnant” condensate containing a fraction of the atoms survived with nearly constant number for more than 1 second and oscillated in a highly excited collective state with the two lowest modes ( $\nu \simeq 2\nu_{axial}$  and  $\nu \simeq 2\nu_{radial}$ ) being predominantly excited. Figure 5 is a plot of the number of remnant atoms  $N_{remnant}$  as a function of  $a_{collapse}$ .

Since  $N_{burst}$  was independent of  $a_{collapse}$  but  $N_{remnant}$  decreased with  $|a_{collapse}|$ , the number of missing atoms increased with  $|a_{collapse}|$ . Interestingly, the number of missing atoms also increased with  $N_0$ , but the fraction of missing atoms versus  $a_{collapse}$  was equal for  $N_0 = 6,000$  and  $N_0 = 15,000$  and was  $\sim 40\%$  for  $|a_{collapse}| < 10 a_0$  and  $\sim 70\%$  for  $|a_{collapse}| \geq 100 a_0$ . The missing atoms were presumably either expelled from the condensate at such high energies that we could not detect them ( $> 20 \mu\text{K}$ ), or they were transferred to untrapped atomic states or undetected molecules.

**Jet formation.** Under very specific experimental conditions, we observed streams of atoms with highly anisotropic velocities emerging from the collapsing condensates. These “jets” are distinguished from the “burst” in that the jets have much lower kinetic energy, in that their velocity is nearly purely radial, and in that they appear only when the collapse is interrupted (i.e., by jumping to  $a_{quench} = 0$ ) during the period of number loss. Collapse processes that were allowed to evolve to completion (until  $N \simeq N_{remnant}$ ) were not observed to emit jets. Examples are shown in Fig. 6 for different  $\tau_{evolve}$  for the conditions of Fig. 1b. The jet size and shape varied from image to image even when all conditions were unchanged, and multi-lobed jets were sometimes observed.

We believe that these jets are manifestations of local “spikes” in the condensate density that form during the collapse and expand when the balance of forces is changed by quenching the collapse. We can estimate the size of the spikes using the uncertainty principle. After a jump to  $a_{quench} = 0$ , the kinetic energy of the atoms in the resulting jet is equal to the confinement energy that the spike had prior to quenching the collapse, i.e.,  $\frac{1}{2}mv^2 = \frac{\hbar^2}{4m\sigma^2}$ , where  $\sigma$  is the width of the spike in the wave function. The anisotropy of the jets indicates that the spikes from which they originated were also highly anisotropic, being narrower in the radial direction. From the widths and the number of atoms in the jets, we can estimate the density in the spikes. Plots of the number of jet atoms and the inferred density in the spikes versus  $\tau_{evolve}$  are presented in Fig. 7. The jets exhibited variability in energy and number that was larger than the  $\sim 10\%$  measurement noise.

#### How well can the theories predict what we see?

Many theories have been developed in an attempt to describe the collapse process. These theories can be distinguished by their differing loss mechanisms, the mechanics of the collapse process, and the origin of the burst atoms. As discussed below, none adequately explain the observed behavior.

One theoretical approach involves three-body losses in regions of the condensate reaching high density. Kagan *et al.*<sup>5</sup> and Saito and Ueda<sup>7</sup> both attack the problem in this way. The models differ in describing the details of the shape of the collapsing condensate, but in both models the maximum “critical” density reached during collapse is determined by a balance between the inward atom flux and the atom loss due to three-body recom-

bination. When three-body losses burn out after removing a large fraction of the atoms, the tight confinement energy of the wave function causes rapid expansion of the condensate. These models have the appealing qualitative features that the expanding condensate may be identified as the burst we observe and the missing atoms might be explained by high-energy atoms that escape by three-body recombination and molecules that we fail to detect.

Comparing our data to these theories relies heavily on the three-body recombination loss coefficient  $K_3$ , which determines the critical density. Like the scattering length,  $K_3$  depends on magnetic field, but it has been predicted<sup>19</sup> to scale as  $K_3 \propto a^4$ .  $K_3$  is small near  $a = 0$  and can only be estimated with a large extrapolation from measurements at larger  $|a|$ . For the most negative  $a_{collapse}$  values that we studied,  $K_3$  has been measured for thermal clouds<sup>20</sup>.

Kagan *et al.*<sup>5</sup> model the collapse by solving the Gross-Pitaevskii equation numerically and assuming that during collapse the BEC contracts until it reaches a critical density of  $n_* = 4\pi\hbar a/mK_3$  at which the three-body loss rate is  $K_3 n_*^2$ . The predicted structure of the collapsing condensate depends on the three-body recombination rate to the trap frequency ( $\xi$  in ref. 5), the BEC is expected to smoothly contract in a single, collective collapse. Kagan *et al.* solve the problem in this regime ( $\xi = 10^{-3}$ ). We can check the plausibility of this model by comparing the predicted and measured burst energies. After three-body loss burns out, the predicted kinetic energy scales as  $E \propto L^{-2} \propto (n_*/N_0)^{2/3}$ , where  $L$  is the condensate width at  $n_*$ . Because of the strong dependence of  $K_3$  on  $a$ ,  $n_*$  should drop sharply with  $a$ ,  $L$  should increase with  $a$ , and  $E$  should thus decrease with  $a$ . However, for  $|a_{collapse}| < 100 a_0$ , we observe that  $E$  increases with  $|a_{collapse}|$ . There is also a large quantitative discrepancy. At  $a_{collapse} = -240 a_0$ , the model underestimates the burst energy by a factor of 20. The burst-energy dependence on  $N_0$  also has the wrong sign, since we observe  $E$  to grow with increasing  $N_0$ . In addition, the model’s prediction for  $\tau_{decay}$  is orders of magnitude too fast, and the predicted scaling with  $a$  and  $K_3$  does not match observations<sup>18</sup>.

Ueda and Huang<sup>6</sup> have shown that under some conditions, the increasing wave function curvature during collapse allows for very sharp local density spikes (“black holes”) to form. Saito and Ueda<sup>7,9</sup> have solved the Gross-Pitaevskii equation numerically using the same basic model as Kagan *et al.* but with a smaller value of the ratio of the recombination rate to the trap frequency ( $\xi \sim 10^{-7}$ ). Their solutions predict the formation of a series of spikes that quickly annihilate themselves through three-body losses to form intermittent microbursts. The energy of the microbursts compares better with our burst data than does one collective collapse. For example, to reach  $n_*$  for 100 atoms at  $-240 a_0$ , the width of the spikes would be  $\sim 80$  nm and the burst energy would be

$\sim 200$  nK.

The microburst scenario also offers a possible explanation for the roughly millisecond burst production time and could also explain the distinction between the burst and remnant atoms. The predicted dependence of the burst energy on scattering length still has the wrong sign for  $|a| < 100 a_0$ , however, and has the wrong  $N_0$  dependence. Neither the Kagan *et al.* nor the Ueda models address the problem of the burst anisotropy.

With an entirely alternative approach, Duine and Stoof<sup>8</sup> assume that inelastic losses are unimportant and model the burst through elastic collisions between BEC atoms. Their model is most applicable to the regime of large  $a_{init}$ , however, so it is still unclear to what extent this model is expected to apply to our measurements<sup>22</sup>. The model predicts a burst anisotropy that increases with increasing initial aspect ratio  $\lambda$  (which disagrees with our measurements<sup>23</sup>), and the predicted burst energies are 2 orders of magnitude lower than what we have observed. Their model also does not account for the missing atoms or the initial flat region in the loss curves like Fig. 1.

**Theoretical Challenges.** Collapsing <sup>85</sup>Rb condensates present a rather simple system with quite dramatic behavior. Theory should be able to explain what we see, but there are major qualitative disagreements between experiment and all of the current theories. Some particularly puzzling results are:

- The decay constant  $\tau_{decay}$  is independent of both  $N_0$  and  $|a_{collapse}|$  for  $|a_{collapse}| < 100 a_0$ , and only weakly depends on these quantities for larger  $|a_{collapse}|$ .
- The burst energy per atom dramatically increases with initial condensate number.
- The number of burst atoms is constant versus  $a_{collapse}$ .
- The number of cold remnant BEC atoms surviving the violent collapse varies between much less and much more than  $N_{cr}$ , depending on  $N_0$  and  $a_{collapse}$ , but the fraction of burst atoms and missing atoms are independent of  $N_0$ .

**Outlook.** From the experimental point of view there remain questions to be answered. For one, is the burst coherent? It may be possible to answer this by generating a sequence of “half bursts” and see if they interfere. For another, where do the missing atoms go? If molecules and/or relatively high-energy atoms are being created, can we detect them?

It is clear that adjustable interactions opens up a fascinating new regime for BEC studies.

---

\* Quantum Physics Division, National Institute of Standards and Technology.

<sup>1</sup> Dalfovo, F., Giorgini, S., Pitaevskii, L. P., & Stringari, S. Theory of Bose-Einstein condensation in trapped gases. *Rev. Mod. Phys.* **71**, 463–512 (1999).

<sup>2</sup> Ruprecht, P. A., Holland, M. J., Burnett, K., & Edwards, M. Time-dependent solution of the nonlinear Schrödinger equation for Bose-condensed trapped neutral atoms. *Phys. Rev. A* **51**, 4704–4711 (1995).

<sup>3</sup> Cornish, S. L., Claussen, N. R., Roberts, J. L., Cornell, E. A., & Wieman, C. E. Stable <sup>85</sup>Rb Bose-Einstein condensates with widely tunable interactions. *Phys. Rev. Lett.* **85**, 1795–1798 (2000).

<sup>4</sup> Roberts, J. L., *et al.*. Controlled collapse of a Bose-Einstein condensate. *Phys. Rev. Lett.* (submitted), (2001).

<sup>5</sup> Kagan, Y., Muryshv, A. E., & Shlyapnikov, G. V. Collapse and Bose-Einstein condensation in a trapped Bose Gas with negative scattering length. *Phys. Rev. Lett.* **81**, 933–937 (1998).

<sup>6</sup> Ueda, M. & Huang, K. Fate of a Bose-Einstein condensate with an attractive interaction. *Phys. Rev. A* **60**, 3317–3320 (1999).

<sup>7</sup> Saito, H. & Ueda, M. Power laws and collapsing dynamics of a trapped Bose-Einstein condensate with attractive interactions. *Phys. Rev. A* **63**, 043601–7 (2001).

<sup>8</sup> Duine, R. A. & Stoof, H. T. C. Explosion of a collapsing Bose-Einstein condensate. *Phys. Rev. Lett.* **86**, 2204–2207 (2001).

<sup>9</sup> Saito, H. & Ueda, M. Intermittent implosion and pattern formation of trapped Bose-Einstein condensates with

an attractive interaction. *Phys. Rev. Lett.* **86**, 1406–1409 (2001).

<sup>10</sup> Sackett, C. A., Gerton, J. M., Welling, M., & Hulet, R. G. Measurements of collective collapse in a Bose-Einstein condensate with attractive interactions. *Phys. Rev. Lett.* **82**, 876–879 (1999).

<sup>11</sup> Gerton, J. M., Strekalov, D., Prodan, I., & Hulet, R. G. Direct observation of growth and collapse of a Bose-Einstein condensate with attractive interactions. *Nature* **408**, 692–695 (2001).

<sup>12</sup> Myatt, C. J., Newbury, N. R., Ghrist, R. W., Loutzenhiser, S., & Wieman, C. E. Multiply loaded magneto-optical trap. *Opt. Lett.* **21**, 290–292 (1996).

<sup>13</sup> The trap frequencies were  $\nu_{radial} = 17.5$  Hz and  $\nu_{axial} = 6.8$  Hz.

<sup>14</sup> Roberts, J. L., Claussen, N. R., Cornish, S. L., & Wieman, C. E. Magnetic field dependence of ultracold inelastic collisions near a Feshbach resonance. *Phys. Rev. Lett.* **85**, 728–731 (2000).

<sup>15</sup> The increase in  $a$  from  $a_{collapse}$  to  $a_{expand}$  is far too rapid to allow for the BEC to expand adiabatically. On the contrary, the smaller the BEC before expansion, the larger the cloud at the moment of imaging. Thus we can readily infer the relative size of the bulk of the BEC just prior to the jump to  $a_{quench}$ .

<sup>16</sup> Pérez-García, V. M., Michinel, H., Cirac, J. I., Lewenstein, M., & Zoller, P. Dynamics of Bose-Einstein condensates: Variational solutions of the Gross-Pitaevskii equations. *Phys. Rev. A* **56**, 1424–1432 (1997).

<sup>17</sup> Beginning at  $a_{init} = +89 a_0$  then jumping to  $a_{collapse} =$

- $-15 a_0$ , we observed  $t_{collapse} = 12(3)$  ms, which is  $\sim 3$  times longer than that measured when beginning at  $a_{init} = 0$  for the same value of  $a_{collapse}$ . ( $n_{init}$  is 6 times lower for  $a_{init} = 89 a_0$  than for  $a_{init} = 0$ ).
- <sup>18</sup> For the range of  $a_{collapse}$  shown in Fig. 2,  $\tau_{decay}$  did not depend on  $a_{collapse}$  or  $N_0$  outside of the experimental noise ( $\sim 20\%$ ). On average,  $\tau_{decay}$  was 2.8(1) ms. For the very negative value of  $a_{collapse} \simeq -250 a_0$ , however,  $\tau_{decay}$  did decrease to 1.8 ms for  $N_0 = 6,000$  and 1.2 ms for  $N_0 = 15,000$ .
- <sup>19</sup> Fedichev, P. O., Reynolds, M. W., & Shlyapnikov, G. V. Three-Body recombination of ultracold atoms to a weakly bound  $s$  level. *Phys. Rev. Lett.* **77**, 2921–2924 (1996).
- <sup>20</sup> For  $a = -240 a_0$ ,  $K_3 = 3 \times 10^{-26} \text{cm}^6/\text{s}$  and for  $a = -310 a_0$ ,  $K_3 = 8 \times 10^{-26} \text{cm}^6/\text{s}^{14}$ . We can set an upper bound of  $K_3 = 10^{-28} \text{cm}^6/\text{s}$  at  $a = 0$  by assuming that the inelastic losses are exclusively three-body. A more realistic estimate of  $K_3 \sim 1 \times 10^{-29} \text{cm}^6/\text{s}$  at  $-30 a_0$  is obtained by assuming that the point of minimum inelastic losses at 172.5 G ( $-144 a_0$ )<sup>14</sup> is the crossover point at which two- and three-body losses are equal, and then scaling the value of  $K_3 = 4 \times 10^{-27} \text{cm}^6/\text{s}$  at  $-144 a_0$  by  $a^4$ . All of the above  $K_3$  estimates are 1/6 of the thermal-cloud values to get the appropriate values for a BEC.
- <sup>21</sup> G. V. Shlyapnikov, Private communication.
- <sup>22</sup> H. T. C. Stoof, Private communication.
- <sup>23</sup> For all of the data in Fig. 4, the initial BEC had an aspect ratio of  $\lambda = 1.6$  before the collapse was induced. When instead we started at  $a_{init} = +100 a_0$ , the BEC was initially more anisotropic ( $\lambda = 2.4$ ), but the burst became more isotropic, with  $E_{ax}$  going up by  $\sim 40\%$  and  $E_{rad}$  dropping by  $\sim 60\%$  for  $N_0 = 15,000$  and  $a_{collapse} = -100 a_0$ .
- <sup>24</sup> Stenger, J., *et al.*. Strongly enhanced inelastic collisions in a Bose-Einstein condensate near Feshbach resonances. *Phys. Rev. Lett.* **82**, 2422–2425 (1999).
- <sup>25</sup> Pattanayak, A. K., Gammal, A., Sackett, C. A., & Hulet, R. G. Stabilizing an attractive Bose-Einstein condensate by driving a surface collective mode. *Phys. Rev. A* **63**, 033604–4 (2001).

**ACKNOWLEDGMENTS.** We extend our thanks to Sarah Thompson for laboratory assistance and to Stephan Dürr, Gora Shlyapnikov, Henk Stoof, Murray Holland, Masahito Ueda, and Rembert Duine for helpful discussions. This research has been supported by the ONR, NSF, ARO–MURI, and NIST. S. L. C. acknowledges the support of a Lindemann Fellowship.

FIG. 1: a. A typical  $a(t)$  sequence. ( $a_0 = 0.529 \text{ \AA}$  is the Bohr radius). The scattering length is jumped at  $t = 0$  in 0.1 ms from  $a_{init}$  to  $a_{collapse}$ , where the BEC evolves for a time  $\tau_{evolve}$ . The collapse is then interrupted with a jump to  $a_{quench}$ , and the field is ramped in 5 ms to a large positive scattering length which makes the BEC expand. After 7.5 ms of additional expansion, the trap is turned off in 0.1 ms and 1.8 ms later the density distribution is probed using destructive absorption imaging with a  $40 \mu\text{s}$  laser pulse (indicated by the vertical bar). The density of the expanded BEC is so low that the rapid transit of the Feshbach resonance pole<sup>24</sup> during the trap turn-off and the subsequent time spent at  $B = 0$  ( $a = -400 a_0$ ) both have a negligible effect. b. The number of atoms remaining in the BEC versus  $\tau_{evolve}$  at  $a_{collapse} = -30 a_0$ . We observed a delayed and abrupt onset of loss. The solid line is a fit to an exponential with a best-fit value of  $t_{collapse} \simeq 3.7(5)$  ms for the delay.

FIG. 2:  $t_{collapse}$  versus  $a_{collapse}$  for  $N_0 = 6000$ . The vertical line indicates  $a_{cr}$  for  $N_0 = 6,000$ . The data were acquired with  $a_{init} = a_{quench} = 0$  (to within  $\sim 2 a_0$ ).

FIG. 3: a. Conceptual illustration of a radial burst focus. b. An image of a radial burst focus taken 33.5 ms after a jump from  $a_{init} = 0$  to  $-30 a_0$  for  $N_0 = 15,000$ .  $T_{rad}/2 = 28.6$  ms, which indicates that the burst occurred 4.9(5) ms after the jump. The axial energy distribution for this burst corresponded to an effective temperature of 62 nK. The image is  $60 \times 310 \mu\text{m}$ . c. Radially averaged cross section of b with a Gaussian fit to the burst energy distribution. The central  $100 \mu\text{m}$  were excluded from the fit to avoid distortion in the fit due to the condensate remnant ( $\sigma = 9 \mu\text{m}$ ) and the thermal cloud ( $\sigma = 17 \mu\text{m}$ ). The latter is present in the pre-collapse sample due to the finite temperature and appears to be unaffected by the collapse. The dashed line indicates the fit to this initial thermal component. Note the offset between the centers of the burst and the remnant. This offset varies from shot to shot by an amount comparable to the offset shown.

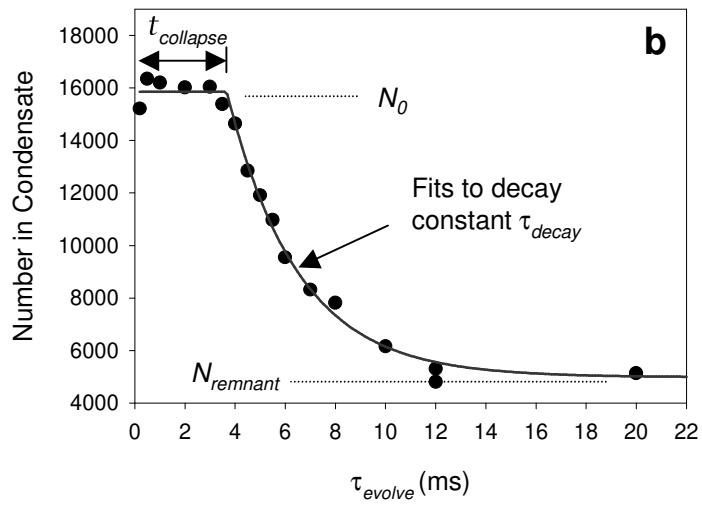
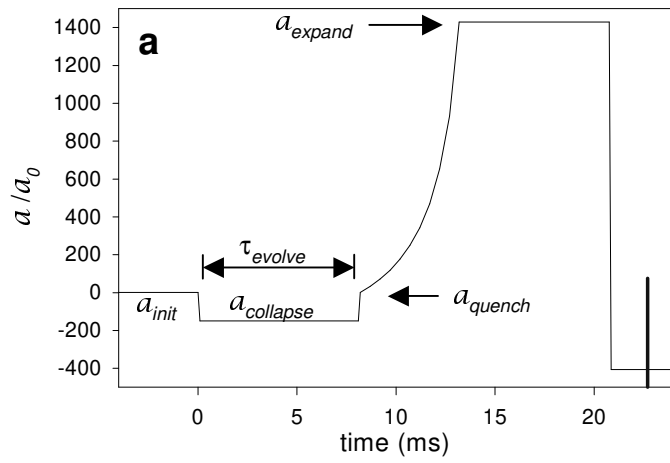
FIG. 4: a. and b. The axial and radial burst energies versus  $a_{collapse}$  for  $N_0 \simeq 6,000$  and  $N_0 \simeq 15,000$ , respectively. The energies were higher for the larger- $N_0$  condensates over the full range of  $a_{collapse}$  studied. The vertical and horizontal error bars indicate the standard error of the measurements and the uncertainty in  $a_{collapse}$  arising from the magnetic-field calibration, respectively. c. The ratio of the radial to the axial energies, which is a measure of the burst anisotropy. For values of  $|a_{collapse}|$  just past  $a_{cr}$ , the burst was isotropic for both  $N_0 \simeq 6,000$  and  $N_0 \simeq 15,000$ . At larger values of  $|a_{collapse}|$ , larger- $N_0$  condensates gave rise to stronger anisotropies<sup>23</sup>.

FIG. 5: a. The average number of remnant atoms versus  $|a_{collapse}|$ . The dashed line is a plot of  $N_{cr}$  based on the measured stability criterion with  $k = 0.46^4$ . When  $N_0$  was 3,000 or 6,000,  $N_{remnant}$  did not exceed  $N_{cr}$ . In contrast, for  $N_0 = 15,000$   $N_{remnant}$  was dramatically higher than  $N_{cr}$  for all four data points. The stability condition in equation (1) determined the collapse point for  $N_0 = 15,000$  but it did not constrain  $N_{remnant}$ . We do not think that the surface-wave excitations<sup>25</sup> are responsible for stabilizing the remnant since we excite large-amplitude breathing modes. Note that for  $N_0 = 6,000$  and  $|a_{collapse}| < 10 a_0$ , more atoms were lost than the number required to lower  $N_{remnant}$  to below  $N_{cr}$ .

FIG. 6: Jet images for a series of  $\tau_{evolve}$  values for the conditions of Fig. 1b. The evolution times were 2, 3, 4, 6, 8, and 10 ms (from a to f). Each image is  $150 \times 255 \mu\text{m}$ . The bar indicates the optical depth scale. An expansion to  $a_{expand} = +250 a_0$  was applied, so the jets are longer than for the quantitative measurements explained in the text. The jets were longest (i.e., most energetic) and contained the most atoms at values of  $\tau_{evolve}$  for which the slope of the loss curve (Fig. 1b) was greatest. A tiny jet is barely visible for  $\tau_{evolve} \simeq 2$  ms (image a), which is 1.7 ms before  $t_{collapse}$ . The images also show how the number of condensate atoms decreases with time. The time from the application of  $a_{quench}$  until the acquisition of the images was fixed at 5.2 ms.

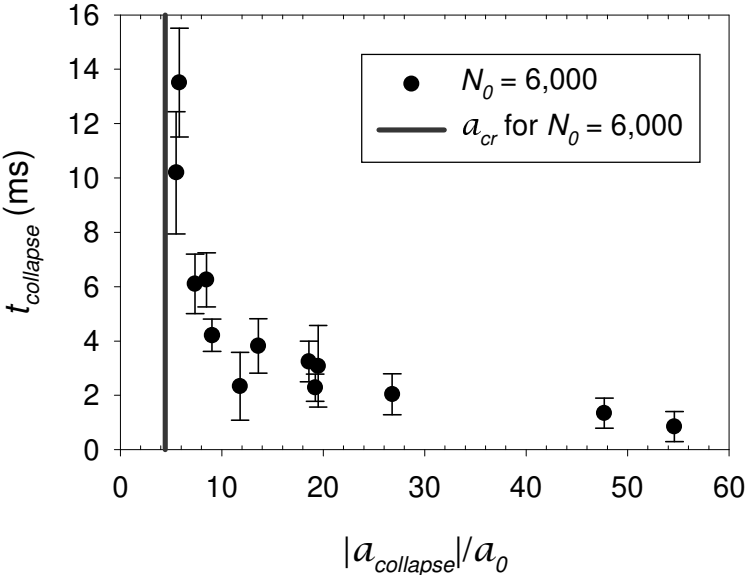
FIG. 7: a. The number of atoms in the jets versus  $\tau_{evolve}$  for the conditions of Fig. 1b. b. The spike density inferred from the kinetic energies of the jets. The bars indicate the range of shot-to-shot variability. For the analysis, we assumed the jets were disk shaped since the magnetic trap is axially symmetric. The images were taken perpendicular to the axial trap axis, viewing the disks edge-on. The jets expanded with  $v \simeq 1$  mm/s, which corresponds to a kinetic energy of  $\sim 6$  nK and a radial pre-quench Gaussian rms width of  $\sim 0.5 \mu\text{m}$ . Since the axial size was below our resolution limit, we could not measure the axial expansion rate. For estimating the spike density, we assumed an axial width equal to the harmonic oscillator length. The atom density in the spikes decreased for larger values of  $|a_{collapse}|$ , and was half as large for  $a_{collapse} = -100 a_0$  as for  $-30 a_0$ .

# Donley, Fig. 1



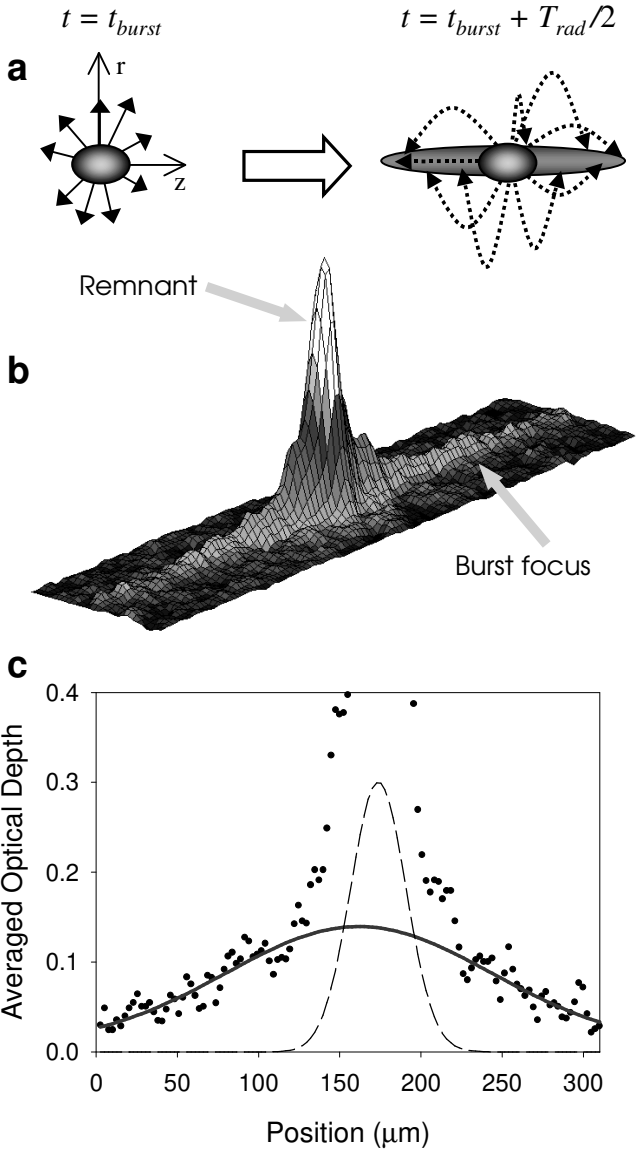


Donley, Fig. 2



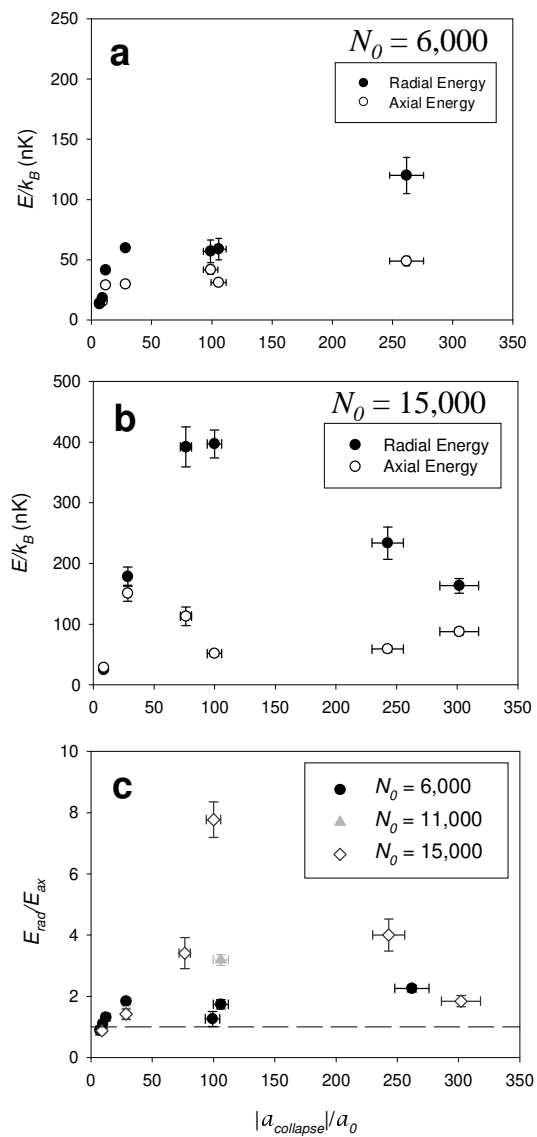


Donley, Fig. 3



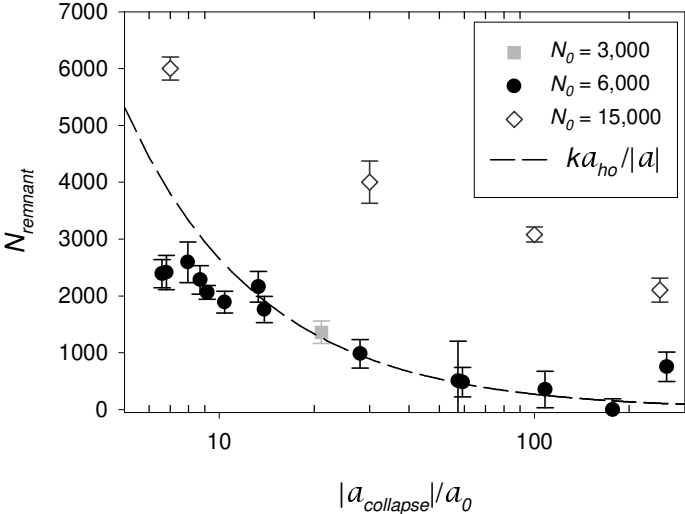


# Donley, Fig. 4



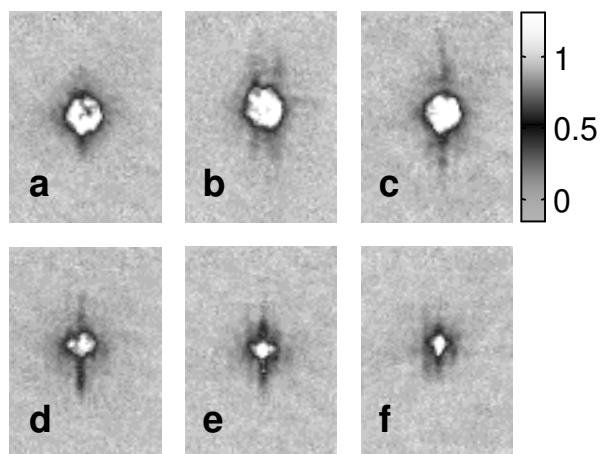


Donley, Fig. 5





# Donley, Fig. 6





# Donley, Fig. 7

